# Dual-Polarized Broadband Array Antenna With BOR-Elements, Mechanical Design and Measurements

Henrik Holter, *Member, IEEE*

***Abstract*—A dual polarized broadband phased array antenna designed for the frequency range 6–18 GHz, a 45° conical grating lobe free scan volume and equipped with BOR-elements developed by Saab is presented. The aim with this array element is to bring about a dual polarized broadband array antenna that is easy to assemble, disassemble and connect to active microwave modules. Disassembling may be important for maintenance and upgrade reasons. Mechanical design and electromagnetic performance in the form of active reflection coefficient, calculated from measured mutual coupling coefficients, and measured active gain element pattern for a central and an edge element is presented. Edge effects in the array, which may be severe in small broadband arrays, are considered in this paper.**

***Index Terms*—Broadband antennas, edge effects, phased array antennas.**

## I. Introduction

THE current progress in advanced radar, electronic warfare and communication systems has lead to a large interest in broadband phased array antennas. The number of published antenna elements usable for broadband arrays is continuously increasing. Some of the up to now most common elements are the tapered slot element (also named Vivaldi-element and notch element) [1], the bunny-ear element [2], [3] and the TEM-horn (single polarized element) [4]. All these elements have a three-dimensional structure. In the last few years, broadband array elements with a two-dimensional structure have also been published. Examples of such elements are given in [5], [6], and [7]. Two-dimensional elements have advantages with respect to manufacturing and conformal mounting. Information regarding electromagnetic properties and design guide lines of arrays with these elements are so far rather limited. Some recently published interesting low-profile broadband elements can be found in [8]–[10].

Broadband arrays are many times difficult to assemble. This is especially true for dual polarized tapered slot arrays, which is probably the most popular broadband array type today. A considerable manufacturing difficulty with dual polarized tapered slot arrays is to obtain the necessary good electrical contact between adjacent elements. Soldering, for example, is many times unpractical. The problem is aggravated in arrays designed to operate at high frequencies because of the small element spacing. If one manages to attach adjacent elements then there is a considerable risk that the array will become one solid piece, which also hinders maintenance. It is possible to design dual polarized bunny-ear arrays without electric contact between adjacent elements. At the presentation of the paper in [3], it was however pointed out that it was necessary to use resistive film from the dipole wings to the ground in order to suppress electromagnetic resonances caused by the gap.

In this paper, a new dual-polarized array element is presented that facilitates the assembling and disassembling process of the array aperture and connecting of the array aperture to microwave modules. A small prototype array with $3 \times 4$ elements was earlier built with the purpose to examine some of the building principles and to compare with numerical calculations [11]. That array was single polarized. The array presented here is dual polarized and has 332 feed points. The array is rather small compared to the wavelength, which makes edge effects important [12]. Edge effects are therefore commented on in this paper.

The paper has been divided as follows. In Section II, electrical and mechanical requirements on the array aperture are presented. In Section III, the electromagnetic design procedure is presented. In Section IV, the mechanical design is presented. Electromagnetic performance of the manufactured array in form active reflection coefficient and embedded element pattern is presented in Section V. Concluding remarks are given in Section VI.

## II. Array Aperture Requirements

The array has been designed for a certain application. This application has set the electrical and physical size requirements on the array aperture. The most important requirements are as follows.

- Frequency range: 6–18 GHz.
- 45° conical scan volume.
- Dual polarization.
- No grating lobes.
- SWR (standing voltage ratio) $< 2$ for the major part of the array elements. This SWR is for a feed line with 50-Ohm characteristic impedance.
- The size of the aperture must be about $16 \times 9$ cm. This size is mainly determined from the requirement on the array beamwidth.

Manuscript received April 18, 2006; revised July 7, 2006. This work was supported by the Swedish Defense Material Administration (FMV).

The author is with Saab Microwave Systems, Stockholm SE-17588 Järfälla, Sweden.

Color versions of one or more of the figures in this paper are available online at http://ieeexplore.ieee.org.

Digital Object Identifier 10.1109/TAP.2006.886557

The requirements on the SWR and grating lobes are for the whole frequency range—scan volume space specified previously. The array elements are connected directly to transmission lines with 50 Ohm characteristic impedance. No additional matching circuits behind the array are allowed. Impedance matching must be achieved directly within the aperture.

From the aforementioned requirements, an element spacing little more than half a wavelength at 18 GHz has been found to be appropriate.

The number of necessary antenna elements is determined by the element spacing, lattice type and the aperture size. A square lattice is used for this array. $17 \times 10$ elements are used for one polarization and $18 \times 9$ elements are used for the other polarization. These numbers are explained shortly. The total number of feed points is therefore 332.

## III. Electrical Design

The electrical design of the array has been performed with the FDTD unit cell numerical code PBFDTD [13]. This software is based on the time domain unit cell technique presented in [14] and is capable of oblique scan angles. Since it is a time domain technique, array data is obtained for all frequencies, for a certain scan angle, in a single computation. This is very convenient for broadband array analysis and design.

As has been pointed out earlier, edge effects may be severe in broadband arrays. Since the array here is rather small, all elements will be affected more or less by edge effects at the lower frequencies. The array design has therefore not only been performed with unit cell analysis where periodic boundaries have been used in both array transversal directions (infinite $\times$ infinite array analysis). Arrays that are finite in one direction and infinite in the other direction have also been analyzed with the PBFDTD code. The required frequency band of operation of the array is 6–18 GHz. In an attempt to reduce the edge effects in the manufactured finite array at the low frequency end of the operational band, the array has instead been designed to operate from 4 GHz.

The final element design has been verified with the commercial Ansoft HFSS finite element based code. Comparisons between the PBFDTD and Ansoft HFSS codes are later presented together with measurements on the manufactured array.

## IV. Mechanical Design

The main goal with the array was to find a mechanical design which makes assembling and disassembling of the array easy. Another important objective was to find a convenient way to connect active modules to the aperture backplane. A description of the mechanical design of the array is presented in this section.

The manufactured array is shown in Fig. 1. It consists of $18 \times 10 = 180$ circular symmetric bullet-like protrusions. Feeds are applied in the gap between each protrusion in both cardinal directions ($x$- and $y$-directions) forming the $x$- and $y$-polarized elements. The number of feed points is, therefore, $17 \times 10$ for one polarization and $18 \times 9$ for the other polarization.

A single protrusion, which thus constitutes a part of two $x$-polarized and two $y$-polarized elements, is shown in Fig. 2. It has an exponential profile and is made of aluminum. For the sake of simplicity, we refer to one protrusion as an element. The length of the element has a major influence on the lower frequency limit. As mentioned earlier, in an attempt to reduce the edge effects at low frequencies, the array was designed to operate from 4 GHz. This has maybe led to an unnecessary long element. The element length is about 1.9 wavelengths at 18 GHz. The element has recently been patented by Saab and has been given the name body of revolution (BOR)-element.

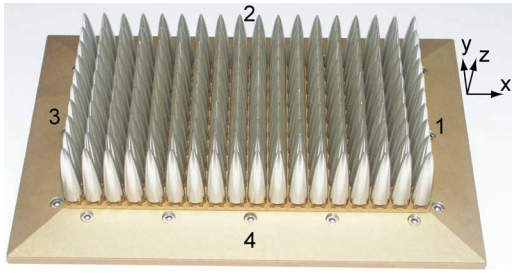


Fig. 1. Manufactured array. The overall size is about $16 \times 9$ cm.

Fig. 2. Antenna element with screw thread.

The ground plane, shown in Fig. 3, is made of aluminum and has grooves in the surface. The purpose of the grooves is to form an electromagnetic open circuit behind each element in a similar manner as the slotline cavity in tapered slot elements [1]. The depth of the grooves has a considerable effect on the array low frequency limit. The antenna elements are screwed into the ground plan. A brick, shown in Fig. 3, is positioned between each element and the ground plane. Two feeding pins, one for each polarization, are attached to each brick. The two feed pins go through holes in the ground plane (forming 50-Ohm coaxial cables) under two of the adjacent antenna elements. The elements are thus fed in the gap between adjacent elements. This feed constitutes an unbalanced to balanced feed for each antenna element. A balanced feed is important for low cross-polarization. A total of only two coaxial feeds are thus needed for one dual polarized element. This is especially important in arrays operating at high frequencies where the element spacing is small, and therefore the available space for connectors, is limited.

The array back plane is shown in Fig. 4. GPO/SMP female blindmate connectors are snapped into specially designed holes in the ground plane. The feeding pins through the ground plane are pressed into the side of the GPO/SMP-connectors attached to the ground plane. This is done after the GPO/SMP connectors have been attached to the ground plane. Standard connectors are

Fig. 3. Array ground plane and bricks with feeding pins.

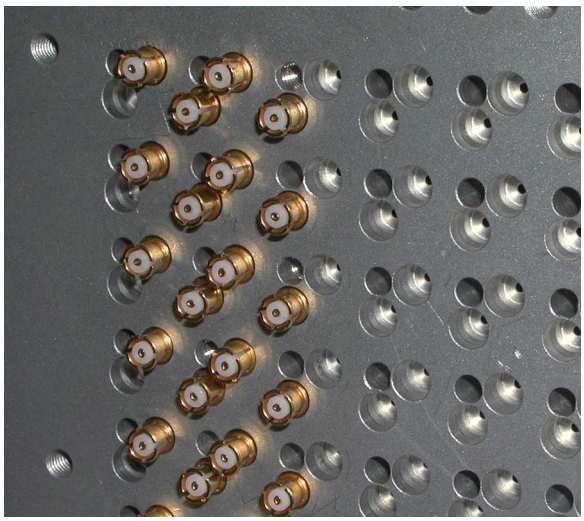

Fig. 4. Backplane with GPO/SMP-connectors.

consequently used. This is an advantage from cost and maintenance points of view.

Microwave modules that fit the connectors on the array backplane have been designed and manufactured, see Fig. 5. The modules are double sided, hermetically sealed, equipped with cooling pipes and are snapped to the connectors on the array back plane. When the modules are detached, it is important that the connectors do not come loose from the array back plane. The connectors are therefore stronger connected to the array back plane than to the modules. This has been accomplished by a suitable shaping of the holes on the array back plane.

A property of this array which does not always apply to other broadband arrays is that after the array has been assembled it can easily be disassembled. That may be important for maintenance and upgrade reasons.

## V. Electrical Performance

Electrical performance in the form of active reflection coefficient and active element pattern for a center and an edge element in the manufactured array is presented in this section. The center element is located close to the center of the array in Fig. 1 and is horizontally ($x$-direction) polarized. The edge element is located close to the middle of edge 4 in Fig. 1 and is also horizontally polarized. For these two elements, the E-plane is the

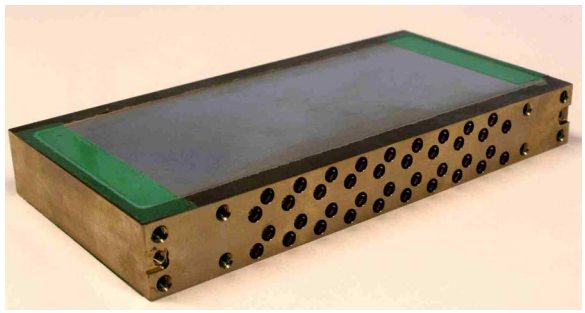

Fig. 5. Microwave module. Nine modules are connected to the array backplane.

$xz$-plane and the H-plane is the $yz$-plane in Fig. 1. The D-plane is the plane between the E- and the H-planes.

### A. Active Reflection Coefficient

The mutual coupling coefficients between the array elements have been measured. The active reflection coefficient has then been calculated from these coefficients (the sum was taken over all the coupling coefficients) for scanning in different planes. A uniform tapering has been used. The magnitude of the active reflection coefficient in linear scale is presented in form of contour plots with frequency (4–18 GHz) on the $y$-axis and scan angle ($-70^\circ$ to $+70^\circ$) on the $x$-axis. Contour lines are given for the values 0.3, 0.5, and 0.7 (to make the plots as readable as possible). The value 0.3 correspond to a SWR of about 1.9, which is close to the requirement of a $\mathrm{SWR} < 2$. This SWR is required for the frequency range 6–18 GHz and for scan angles up to 45° in all planes. A dashed rectangle has been inserted in each contour plot to indicate this region.

The active reflection coefficient for scan in the E-plane, H-plane, and the D-plane (diagonal plane) for the center element is shown in Figs. 6–8. Edge element active reflection coefficient for scan in the E-plane and the H-plane is shown in Figs. 9 and 10. SWR (calculated from measured coupling coefficients via the active reflection coefficient) for broadside and $+45^\circ$ scan in the E- and H-planes for the center element is shown in Figs. 11–13. Also shown in these figures are the PBFDTD and Ansoft HFSS calculated SWR (with infinite $\times$ infinite array unit cell analysis). These plots correspond to a single scan angle in Figs. 6–8.

A number of observations based on the plots are given here.

The reflection coefficient within the dashed rectangle in the contour plots is lower than 0.3 for most of the points. There are also "islands" with higher values.

The edge element, Figs. 9 and 10, is performing rather well despite that it is located close to the array edge and, therefore, especially exposed to edge effects. The polarization of this element is parallel to the adjacent array edge. An element, not shown here, positioned close to array edge 3 in Fig. 1 and polarized in a direction orthogonal to the array edge performs a little bit worse. This is probably caused by the fact that the measured mutual coupling coefficients are stronger in the E-plane than the H-plane for closely located elements. Since a transmitting element, with a strong mutual coupling coefficient, outside the array edge is "missing" in the finite array (as compared with

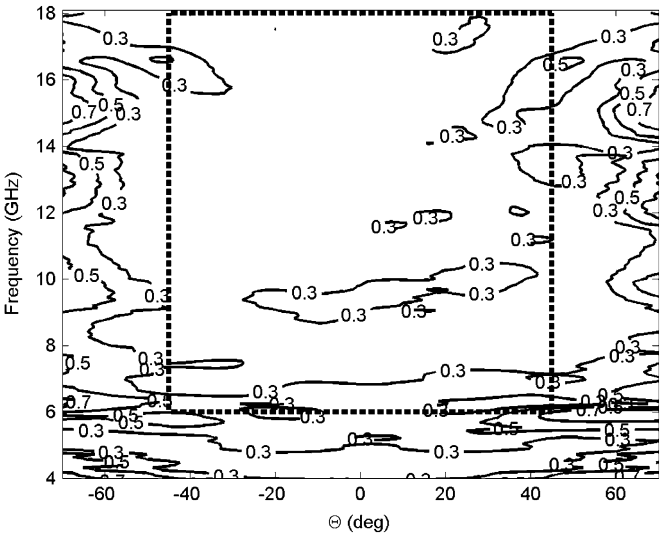


Fig. 6. Active reflection from measured coupling coefficients. E-plane scan. Center element.

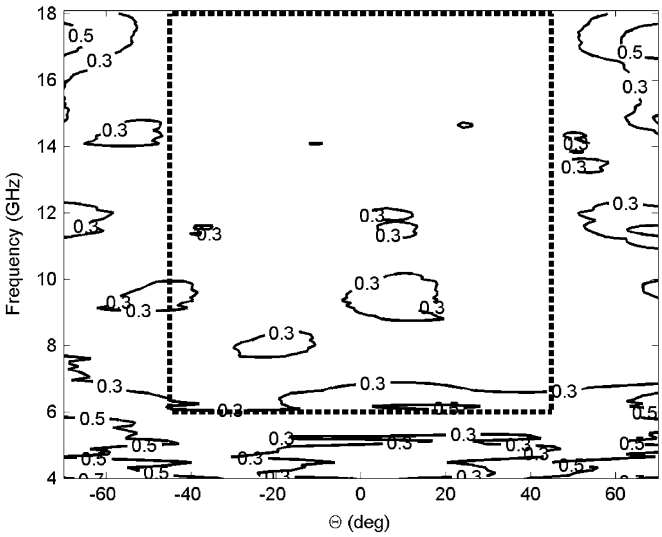


Fig. 7. Active reflection from measured coupling coefficients. H-plane scan. Center element.

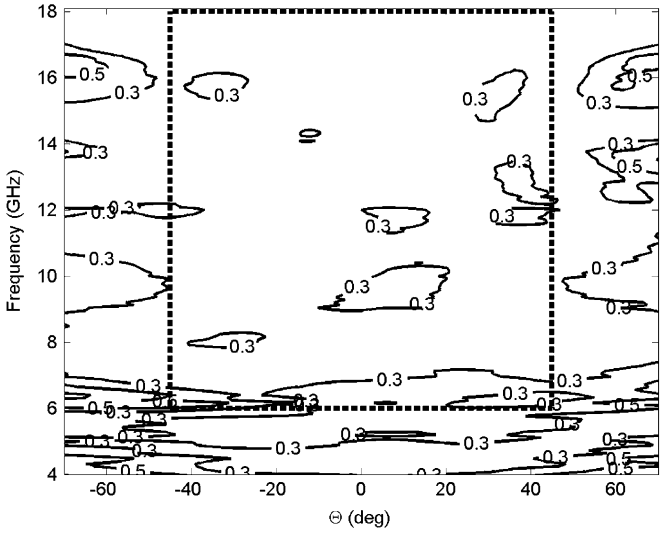


Fig. 8. Active reflection from measured coupling coefficients. D-plane scan. Center element.

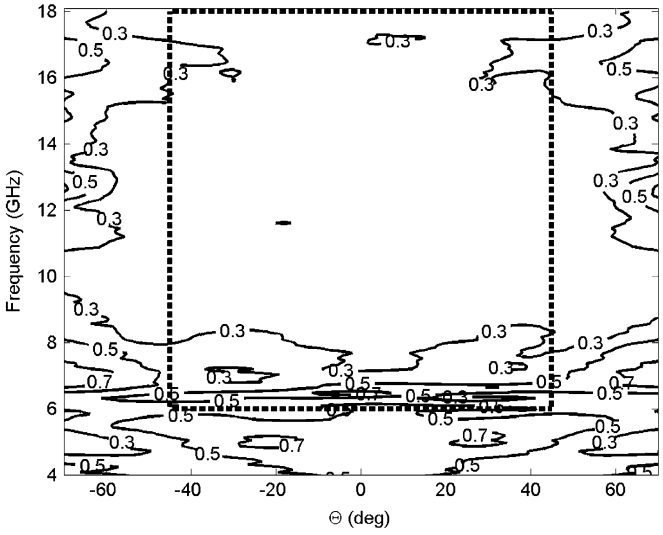


Fig. 9. Active reflection from measured coupling coefficients. E-plane scan. Edge element.

the infinite array) when the active reflection coefficient is calculated for the edge element, the effect on the active reflection coefficient will be substantial.

There seems to be several broad peaks in Figs. 11–13. It is reasonable to assume that the peaks are caused by edge reflections. For broadside scan (Fig. 11), reflections from all four edges are plausible, which complicates the appearance of the peaks. However, when scanning to fairly large angles in one of the principal planes (E- or H-plane), it may be that the peaks are dominated by reflections from the two array edges that are orthogonal to the scan plane. If this is the case, the peaks should occur when the width of the array in the direction that coincides with the scan plane is about a multiple of half a wavelength. This means that the peaks should then be spaced about 0.96 GHz for E-plane scan and 1.7 GHz for H-plane scan. The number of peaks in the frequency interval 6–18 GHz should therefore be about 12 for E-plan scan and 7 for H-plane scan. A glance at Figs. 12 and 13 indicate that this may be the case. Since some of the peaks in the plots are rather wide, they may be composed of two adjacent peaks. Edge effects in arrays, especially broadband arrays with strong mutual coupling at the lower end of the frequency band because of the small element spacing, is a complicated phenomenon that has been investigated by several authors; see, for example, [12] and [15]–[18].

There are $17 \times 10$ array elements with the same polarization as the center element. Since there are 10 elements in one of the direction, the center element is not positioned exactly at the center of the array. But since it is positioned close to the array center, there is a left-right symmetry in Figs. 6–8. For the edge element, Figs. 9 and 10, there is, as expected, symmetry for E-plane scan but not for H-plane scan.

The element spacing has been chosen to avoid grating lobes for scan angles up to 45° in all scan planes. It can be observed

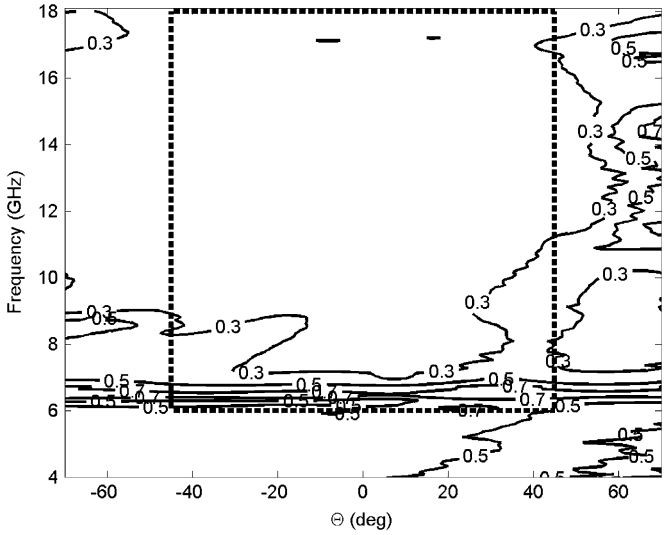


Fig. 10. Active reflection from measured coupling coefficients. H-plane scan. Edge element.

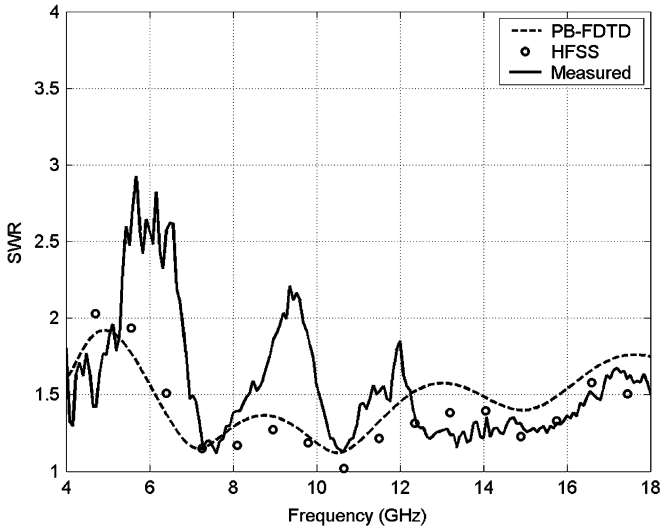


Fig. 11. SWR for a center element from measured coupling coefficients and calculated ($\infty \times \infty$ array). Broadside scan.

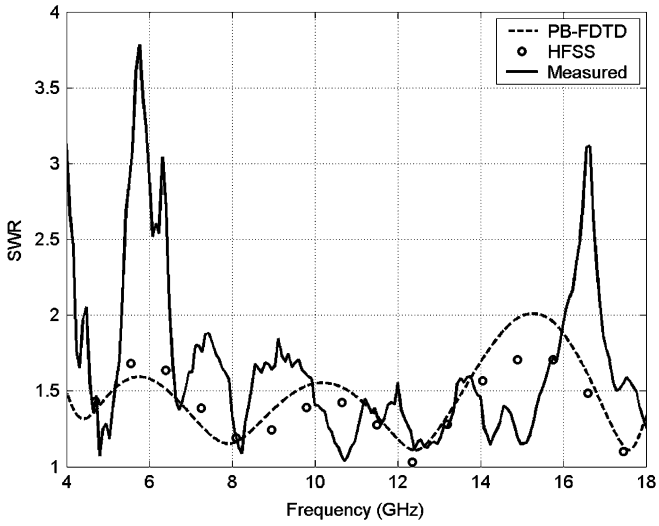


Fig. 12. SWR for a center element from measured coupling coefficients and calculated ($\infty \times \infty$ array). E-plane $+45^\circ$ scan.

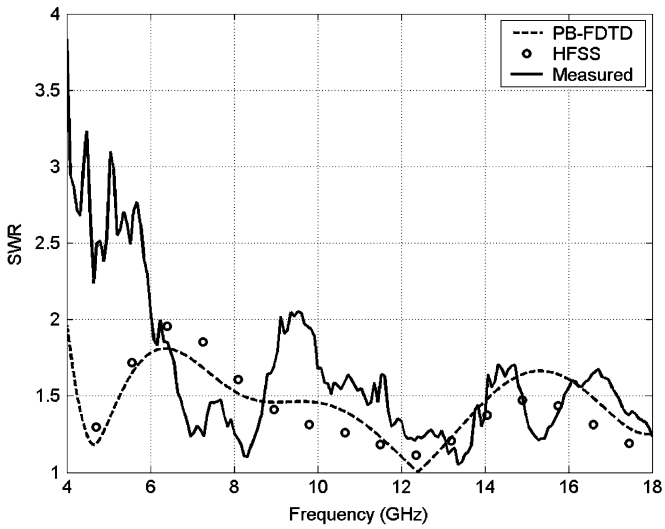


Fig. 13. SWR for a center element from measured coupling coefficients and calculated ($\infty \times \infty$ array). H-plane $+45^\circ$ scan.

in the contour plots that for scan angles larger than 45° the reflection coefficient has a tendency to increase as the frequency increases. This is most likely caused by the first grating lobe, which, because of the finiteness of the array, becomes more and more visible as the frequency increases.

### *B. Embedded Element Pattern*

In this section, measured embedded element pattern for the same center and edge element as dealt with before is presented. The embedded pattern is the pattern of a single element in the array when all other elements are terminated in matched loads. The patterns are normalized with the theoretical infinite ideal array element gain pattern [15]

$$g_e(\theta,\varphi,\lambda)] = \frac{4\pi A}{\lambda^2}\left(1-\left|\Gamma_A(\theta,\varphi,\lambda)\right|^2\right)\cos\theta \qquad (1)$$

where $\lambda$ is the wavelength, $A$ is the unit cell area, $(\theta,\varphi)$ is the scan angle in a spherical coordinate system where the $z$-axis is parallel to the array normal direction and $\Gamma_{\mathrm{A}}$ is the active reflection coefficient. When (1) is used for normalization in this paper, $\Gamma_{\mathrm{A}}$ has been set equal to zero, which results in the "ideal element pattern." Another name for embedded element pattern is "scan element pattern" [20]. The confusing but widespread name "active element pattern" is not used here, also see [20]–[22].

Figs. 14–17 show with (1) normalized contour plots of measured embedded element pattern in the E- and H-plane. A positive (negative) value in the plots means that the measured element gain is higher (lower) than the gain pattern calculated from (1). A dashed rectangle inserted into the plots indicates as earlier the design area.

A number of observations based on the plots in Figs. 14–17 are given later.

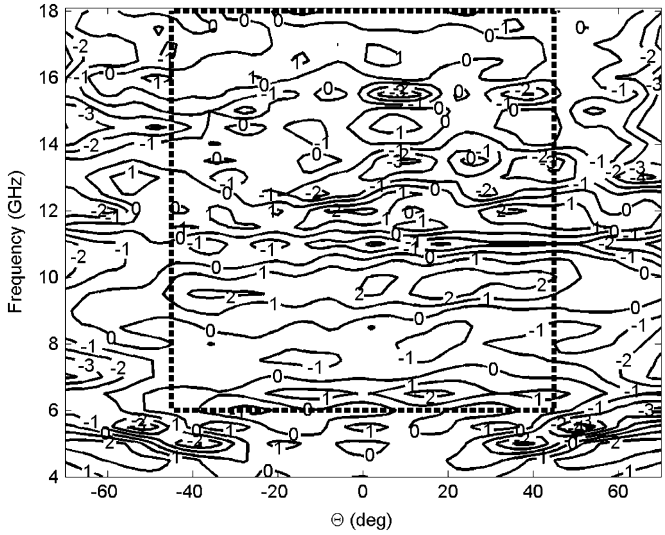


Fig. 14. Measured normalized embedded element pattern (dB). E-plane. Center element.

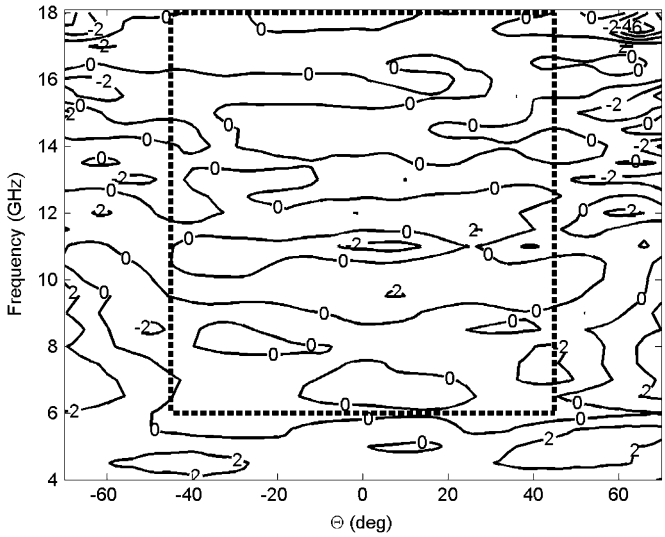


Fig. 15. Measured normalized embedded element pattern (dB). H-plane. Center element.

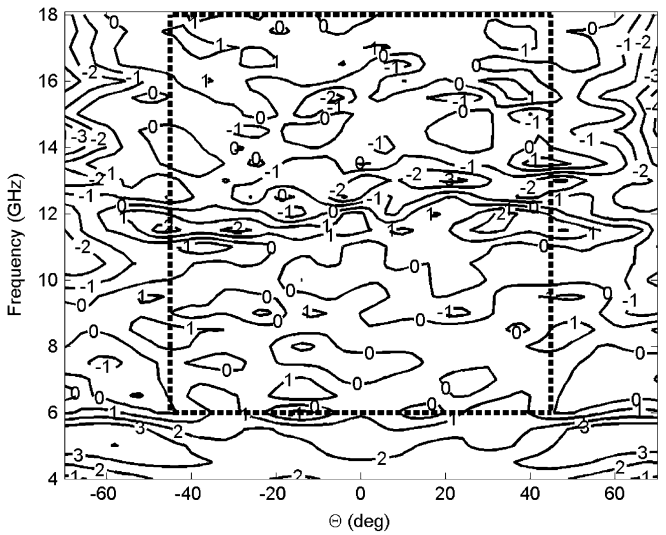


Fig. 16. Measured normalized embedded element pattern (dB). E-plane. Edge element.

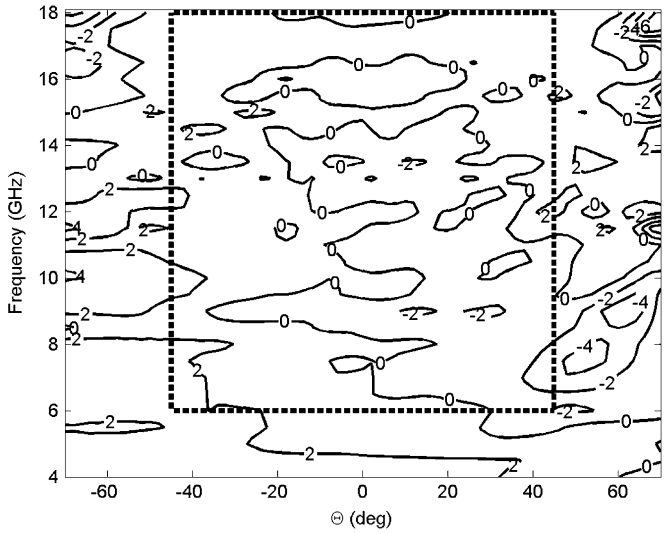


Fig. 17. Measured normalized embedded element pattern (dB). H-plane. Edge element.

The fluctuations in the plots are larger for E-plane scan than for H-plane scan. That may be explained by the fact that the measured mutual coupling coefficients between the center element and elements close to this element are stronger in the E-plane than in the H-plane.

If (1) is a very good approximation, then the plotted quantity in Figs. 14 and 15 for the center element should be near zero dB. That is almost the case as can be seen. On average, the values are just above zero, which shows that the measured element gain pattern, on average, is somewhat higher than the ideal element gain pattern calculated from (1). Equation (1) should be a better approximation at higher frequencies since the array then becomes electrically larger and the edge effects are less pronounced. That also seems to be the case in the figures.

Measured element pattern for the edge element in the E- and H-plane is shown in Figs. 16 and 17. The edge element is positioned close to the middle of edge 4 in Fig. 1. H-plane scan is performed in the $yz$-plane, which is orthogonal to this edge. That explains the nonsymmetry around the $\theta = 0^\circ$ point. Negative $\theta$-values in Fig. 17 correspond to scanning in the $yz$-plane with $y$ negative (see Fig. 1). The plotted quantity in Fig. 17 is on average higher for negative than for positive $\theta$-values. This is expected since the measured active element pattern does not follow the approximate cos $\theta$-behavior as in (1) for negative $\theta$-values [(1) is valid only for infinite arrays or approximately valid for center elements in large arrays]. For E-plane scan (Fig. 16) there is as expected more symmetry around the $\theta = 0^\circ$ point.

Measured cross-polarization in the E- and H-plane is shown in Figs. 18 and 19. The cross-polarization level is similar to the cross-polarization level in a $16 \times 16$ element dual polarized tapered slot array earlier built at Saab and similar to the measured cross-polarization level presented in [2] and [23].

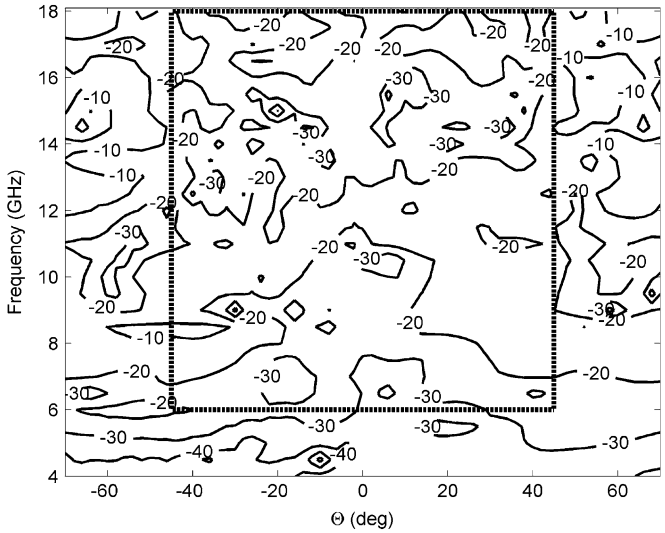


Fig. 18. Measured cross-polarization (dBi) of mbedded element pattern. E-plane. Center element.

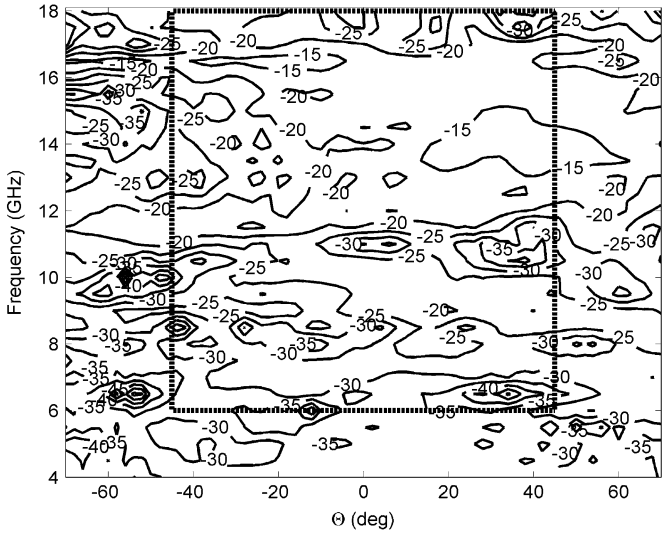


Fig. 19. Measured cross-polarization (dBi) of embedded element pattern. H-plane. Center element.

## VI. Conclusion

A dual polarized broadband array that is easy to manufacture and to connect to microwave modules has been presented.

The edge effects observed in the manufactured array are less severe than expected. This may partially be explained by the fact that not only infinite $\times$ infinite array analysis was performed in the design process. Also, infinite $\times$ finite array analysis was performed.

There are no dielectric materials in the array. It is completely made of metal. There will therefore be no dielectric losses. Conducting losses are negligible.

Tapered slot arrays can, as shown in [24], suffer from electromagnetic resonances in the dielectric material the elements are made off. A technique to eliminate the resonances is presented in [24]. A huge number of numerical calculations based on unit cell analysis, has never shown any hint that there may be resonances in arrays with BOR-elements.

The elements are made of solid aluminum. This is appropriate for the array here, since the elements are small. If BOR-elements are going to be used for arrays operating at lower frequencies they can be made of metalized plastic or be made hollow in order to reduce the weight.

## Acknowledgment

The author would like to thank the following people for contributing to this work: J. Grabs, K. Åsberg, R. Gustafsson (all at Saab Avitronics), and J. Eriksson at Saab Bofors Dynamics.

## References

[1] J. Shin and D. H. Schaubert, "A parameter study of stripline-fed Vivaldi notch-antenna arrays," *IEEE Trans. Antennas Propag.*, vol. 47, no. 5, pp. 879–886, May 1999.

[2] J. J. Lee, S. Livingstone, and R. Koenig, "A low profile wide-band (5:1) dual-pol array," *IEEE Antennas Wireless Propag. Lett.*, vol. 2, pp. 46–49, 2003.

[3] J. J. Lee, S. Livingstone, and R. Koenig, "Performance of a wideband (3–14) GHz dual-pol array," in *IEEE Int. Antennas Propag. Symp. Dig.*, Jun. 2004, vol. 1, pp. 551–554.

[4] D. T. McGrath and C. E. Baum, "Numerical analysis of planar bicone and TEM horn antennas," in *IEEE Int. Antennas Propag. Symp. Dig.*, Jun. 1997, vol. 35, pp. 1058–1061.

[5] B. Munk, "A low-profile broadband phased array antenna," in *IEEE Int. Antennas Propag. Symp. Dig.*, Jun. 2003, vol. 41, pp. 448–451.

[6] B. Thors, H. Steyskal, and H. Holter, "Broadband fragmented aperture phased array element optimization using genetic algorithms," *IEEE Trans. Antennas Propag.*, vol. 53, no. 10, pp. 3280–3287, Oct. 2005.

[7] B. Thors and H. Steyskal, "Synthesis of planar broadband phased array elements with a genetic algorithm," in *Proc. Antenna Appl. Symp.*, Sep. 2005, pp. 324–344.

[8] M. W. Elsallal and D. H. Schaubert, "Reduced-height array of balanced antipodal Vivaldi antennas (BAVA) with greater than octave bandwidth," in *Proc. Antenna Appl. Symp.*, Sep. 2005, pp. 226–242.

[9] A. Neto and J. J. Lee, "Ultrawide-band properties of long slot arrays," *IEEE Trans. Antennas Propag.*, vol. 54, no. 2, pp. 534–543, Feb. 2006.

[10] J. J. Lee, S. Livingstone, R. Koenig, D. Nagata, and L. L. Lai, "Compact light weight UHF arrays using long slot apertures," *IEEE Trans. Antennas Propag.*, vol. 54, no. 7, pp. 2009–2015, Jul. 2006.

[11] H. Holter, "A new type of antenna element for wide-band wide-angle dual polarized phased array antennas," in *Proc. IEEE Int. Symp. Phased Array Syst. Tech.*, Oct. 2003, pp. 393–398.

[12] H. Holter and H. Steyskal, "On the size requirement for finite phased array models," *IEEE Trans. Antennas Propag.*, vol. 50, no. 6, pp. 836–840, Jun. 2002.

[13] PBFDTD commercial code developed by H. Holter.

[14] H. Holter and H. Steyskal, "Infinite phased-array analysis using FDTD periodic boundary conditions—Pulse scanning in oblique directions," *IEEE Trans. Antennas Propag.*, vol. 47, no. 10, pp. 1508–1514, Oct. 1999.

[15] R. C. Hansen, "Anomalous edge effects in finite arrays," *IEEE Trans. Antennas Propag.*, vol. 47, no. 3, pp. 549–554, Mar. 1999.

[16] C. Craeye and M. Arts, "Modulated oscillations in the scan impedance of a finite phased array," *IEEE Trans. Antennas Propag.*, vol. 51, no. 9, pp. 2504–2506, Sep. 2003.

[17] C. Craeye, A. G. Tijhuis, and D. Schaubert, "An efficient MoM formulation for finite-by-infinite arrays of two-dimensional antennas arranged in a three-dimensional structure," *IEEE Trans. Antennas Propag.*, vol. 52, no. 1, pp. 271–282, Jan. 2004.

[18] C. Craeye and X. Dardenne, "Element pattern analysis of wide-band arrays with the help of a finite-by-infinite array approach," *IEEE Trans. Antennas Propag.*, vol. 54, no. 2, pp. 519–526, Feb. 2006.

[19] N. Amitay, V. Galindo, and C. P. Wu, *Theory and Analysis of Phased Array Antennas*. New York: Wiley-Interscience, 1972.

[20] R. C. Hansen, *Phased Array Antennas*. New York: Wiley, 1988, p. 2.

[21] D. M. Pozar, "The active element pattern," *IEEE Trans. Antennas Propag.*, vol. 42, no. 8, pp. 1176–1178, Aug. 1994.
[22] R. C. Hansen, "Comments on "The active element pattern"," *IEEE Trans. Antennas Propag.*, vol. 43, no. 6, pp. 634–634, Jun. 1995.
[23] C. Hemmi, R. T. Dover, F. German, and A. Vespa, "Multifunction wide-band array design.," *IEEE Trans. Antennas Propag.*, vol. 47, no. 3, pp. 425–431, Mar. 1999.
[24] H. Holter, T.-H. Chio, and D. Schaubert, "Elimination of impedance anomalies in single- and dual-polarized endfire tapered slot phased arrays," *IEEE Trans. Antennas Propag.*, vol. 48, no. 1, pp. 122–125, Jan. 2000.

**Henrik Holter** (M'04) received the M.Sc.E.E. degree (with the distinction "Best Graduate of the Year") and the Ph.D. degree in electromagnetic theory from the Royal Institute of Technology, Stockholm, Sweden, in 1996 and 2000, respectively.

He is currently with the R&D sensor section at Saab Microwave Systems, Stockholm, Sweden, working on array antennas, low signature antennas and other types of antennas. From 1986 to 1996, he served the Swedish Navy with a Captain degree. He is author of about 35 journal and conference publications in the area of broadband array antennas.

Dr. Holter received the IEEE Antennas and Propagation Society 2003 R. W. P. King Award in 2004.